Received: 11 March 2019 | Revised: 23 July 2019 | Accepted: 3 August 2019

DOI: 10.1002/jrs.5728

RESEARCH ARTICLE

WILEY Journal of RAMAN SPECTROSCOPY

A surface-enhanced Raman-spectroscopic study: Verification of the interparticle gap dependence of field enhancement by triangulation of spherical gold nanoparticle trimers

Katharina Dort | **Kathrin Kroth** | **Peter J. Klar**

Institute of Experimental Physics I and Center for Materials Research (ZfM/LaMa), Justus Liebig Unversity, Gießen, Germany

Correspondence
Peter J. Klar, Institute of Experimental Physics I and Center for Materials Research (ZfM/LaMa), Justus Liebig Unversity, Heinrich-Buff-Ring 16, 35392 Gießen, Germany.
Email: Peter.J.Klar@exp1.physik.uni-giessen.de

Abstract

Strong electric field enhancement in the interparticle gap of resonators formed by two spherical Au nanoparticles occurs for polarization of the incoming light parallel to the dimer axis. This enhancement exhibits a strong dependence on gap width and is the basis of surface-enhanced Raman scattering or tip-enhanced Raman scattering. The enhancement factor as a function of gap width can be readily calculated solving Maxwell's equations. However, the derived dependence is difficult to verify experimentally, in particular, because of the large uncertainty in determining the interparticle gap value, which is typically one or two orders of magnitude smaller than the diameters of the Au spherical nanoparticles forming the resonator. We demonstrate that a much more reliable verification of the predicted interparticle gap dependence of the electric field enhancement is possible using an approach analogous to triangulation in surveying and mapping.

KEYWORDS

distance determination, electric field enhancement, plasmonics, polarization dependence, SERS

1 | INTRODUCTION

The enhancement of Raman scattering in the presence of metal nanoparticles, commonly known as surface-enhanced Raman scattering (SERS), results from the coupling of Raman-active molecules to surface plasmons in the metal particles[1] and reflects the antenna action of the arrangement of metal nanoparticles with respect to the incoming and emitted or scattered light field. Today, the effect is already exploited in a variety of applications, for example, in chemistry, biophysics, or medicine.[2–4] Raman-enhancement factors up to 10^{14} have been reported enabling even single-molecule detection by SERS.[5,6]

The SERS effect is particularly strong in the gap region between two adjacent metal nanoparticles forming a dimer. Such hot spots[7] arise due to the coupling of the localized surface plasmons of the adjacent nanoparticles forming the dimer. The polarization of the incident field determines the strength of the plasmon–plasmon interaction[8,9] and consequently also the magnitude of the SERS signal.[10] The interaction and, thus, also the field enhancement are strongest for the polarization of the light field parallel to the dimer axis. The electric field

distribution between the metal nanoparticles may be readily calculated on the basis of Maxwell's equations. Additional quantum effects may need to be considered for gap widths below ~1 nm.[11] Arrangements of more than two metal nanoparticles also exhibit localized hot spots in the smallest gaps between the particles.[12]

Electric field enhancement and Raman enhancement are not the same, though often synonymously used. The Raman enhancement achieved, in contrast to the field enhancement, depends not only on the resonator or antenna structure but also on the Raman cross sections of the molecules as well as their orientation inside the hot spot or attached to the nanoparticles' surfaces.[13] The dependence of the Raman cross sections of the molecule on excitation wavelength is determined to a large extent by its electronic structure and resonances of the excitation light with electronic transitions.[14] Thus, changes of the molecule's electronic structure introduced by its attachment to the metal surface may also alter the Raman response in addition to the electric field enhancement caused by the antenna structure. Such chemical contributions to SERS are still heavily disputed and difficult to assess in the analysis of experimental data as well as in theoretical modelling. Furthermore, it is worth noting that the Raman-active species may exhibit modes of different symmetry reflected by different Raman tensors of the modes. These, in turn, lead to a dependence of the Raman intensity on the directions of the polarizations of incoming and scattered light with respect to the molecule orientation. For example, Raman signals of modes of different symmetry exhibit, as a consequence, different depolarization ratios in spectra obtained from randomly oriented molecules in solution.[15,16] Corresponding situations for Raman scatterers in the hot spot of dimer structures that exhibit an anisotropic field enhancement have not been analyzed to our knowledge.

The electric field enhancement of a dimer hot spot strongly varies with the gap width between the nanoparticles forming the dimer. Accordingly, the distance between the nanoparticles will have a crucial impact on the enhancement of the Raman signal.[17] Validations concerning the theoretical predictions[9] of the distance dependence of electric field enhancement are very challenging, as a precise measurement of the gap between adjacent nanoparticles is merely impossible and prone to large experimental uncertainties. The reason is that the diameters of the nanoparticles involved are typically in the range of about 100 nm, whereas the gaps of interest are in the range of a few nanometers only. Tip-enhanced Raman spectroscopy (TERS), on the other hand, can provide precise distance information[18–20] but requires a thin layer of Raman-active molecules. Depending on the molecule under investigation, this can be experimentally challenging. Furthermore, typically, the Raman enhancement of such resonator structures is measured, whereas the electric field enhancement is simulated. A simulation of the full Raman enhancement would require precise knowledge of the modifications of the Raman cross sections and the electronic structure of the molecule, which arise from its interaction with the metal surface. These circumstances make it difficult to verify the theoretical predictions.

Our approach of verifying the theoretically predicted gap dependence of the electric field enhancement is inspired by triangulation used in surveying and mapping. It allows us to separate to a large extent the gap width dependence of the electric field enhancement from the additional factors related to employing Raman spectroscopy as a probe. We study the Raman response of triangular arrangements of spherical gold nanoparticles, so called trimers, which are homogeneously coated with a Raman-active dye. The geometrical arrangement, in particular, the angles between the legs of the triangle formed by connecting the centers of the spheres as well as the spheres' radii can be readily determined from SEM images. The Raman response of the trimer is dominated by the three hot spots formed between the three spherical gold particles. We perform Raman measurements using linearly polarized light for excitation and detect the scattered light of the same polarization in back-scattering geometry. Detecting the mode intensities exhibits characteristic variations as a function of angle between a selected characteristic trimer axis and the polarization. The intensities as a function of angle can be fitted using an angle response given by a superposition of independent contributions from the three hot spots of the trimer. The magnitudes of these three enhancement factors are related to the triangular arrangement of the nanoparticles forming the trimer. In the fitting, the enhancement factors of the three gaps are taken from a theoretical dependence of electric field enhancement versus interparticle gap width derived by finite element simulations and serving as master curve. Furthermore, it is assumed that all gaps scale by the same scaling factor, that is, that the shape of the triangle is known and only similar triangles are considered in the fitting of the experimental data. This approach is based on a set of assumptions that are verified in the course of the work: (a) The dye molecules inside the hot spots are arranged at random, and the Raman enhancement of all modes in the chosen polarization geometry shows a dominating characteristic E^4 dependence[21] independent of mode symmetry, where E is the component of the electric field parallel to the axis through the center of the two nanoparticles forming the gap; and (b) the Raman enhancement of the trimer as a whole is given by the sum of the contributions of its three hot spots, that is, the response of one hot spot is not affected by the response of the two others.

The paper is structured as follows: The experimental and simulation methods used are summarized in Section 2. We study the polarization-dependent Raman response of dimers theoretically and experimentally in Section 3. In particular, we focus on the angle-dependent intensity behavior of Raman-active modes of different symmetry and prove that it is the same for all modes when the molecules are oriented randomly inside the hot spot. On the basis of the results obtained for the dimer, we analyze in Section 4 the angle-dependent Raman data of more than 10 trimers and, thus, verify the simulated master curve of the electric field enhancement as a function of gap width of the hot spot.

2 | METHODS

2.1 | Sample preparation

Nanoparticle arrangements consisting of two or three spherical gold nanoparticles with a diameter of about 250 nm were realized by combining top-down nanofabrication with self-assembly of nanoparticles. In a first step, nanometer-sized cavities with diameters of about 0.5 μm were fabricated in a 450 nm thick polymethyl methacryate (PMMA) layer on a (100) silicon substrate by electron-beam lithography. These cavities define the positions where the nanoparticle arrangements of interest will be formed. Each cavity is located in the center of a marker structure consisting of four line openings, 4 μm in length and 0.6 μm wide, which point in a cross-like arrangement towards the center. The inner edges of the line openings are 10 μm away from the center. The marker structure is essential for defining a selected characteristic axis giving the orientation of the nanoparticle arrangement at the position of the cavity with respect to the marker structure. Similarly, the marker structure serves as an orientation in the Raman microscopic study and allows one to define the orientation of the linear polarization direction of the excitation light with respect to the marker structure and, thus, with respect to the selected characteristic axis of the nanoparticle arrangement studied.

The cavities and the line openings of the marker structure are filled with spherical gold nanoparticles employing the menicus-force deposition method in a second preparation step. The menicus-force deposition method relies on a self-assembly process.[22] For this, an aqueous gold nanoparticle suspension is deposited between the structured PMMA surface and a cover plate. The cover plate is driven by a stepper motor at a defined speed and moves parallel to the structured PMMA surface.[23,24] Thus, the meniscus of the suspension between coverplate and PMMA surface moves at the same speed across the structured surface. At the mensicus, the nanoparticles are pushed into the cavities and into the line openings of the marker structure by the capillary force acting at the air-suspension-substrate three-phase contact line. The size and shape of the cavities, concentration of the nanoparticles in the suspension, and the speed of the cover plate determine the number and arrangement of nanoparticles inside the cavity. For the samples shown in the following sections an aqueous Au-nanoparticle suspension with a concentration of 7.2×10^8 particles/ml and a speed of approximately 1.3 mm/hr for the cover plate turned out to be optimally suited.

Scanning electron microscopy (SEM) images of nanoparticle arrangements consisting of three (left-hand side) and two (right-hand side) spherical gold nanoparticles, that is, a trimer and a dimer, are shown in Figure 1. The line openings of the marker structure surrounding the nanoparticle arrangement are also filled with nanoparticles and clearly visible in the SEM image as well as under an optical microscope.

In a third step, the PMMA film is removed from the silicon wafer after the nanoparticles are assembled by immersing the sample in acetone for at least 6 hr. In the final step, the entire substrate is immersed in a 0.25 mM methylene blue (MB) water solution for 12 hr. MB consists of the organic cation 3,7-bis(dimethylamino)phenothiazin-5-ium $(C_{16}H_{18}N_3S)^+$ and the anion Cl^-.

2.2 | Raman spectroscopy

The Raman spectra are recorded at room temperature in a back-scattering geometry using a Renishaw in Via Raman spectrometer combined with a Leica optical microscope. A He-Ne laser with an emission wavelength of 632.8 nm serves as excitation source. The laser power is set to 2 μW and the diameter of the laser spot is approximately 3 μm. A 50× objective (Leica, NA = 0.75) is used to focus the linearly polarized laser light onto the sample. A rotatable $\lambda/2$ plate is added to the optical path in order to tune the orientation of the polarization direction of the incoming and scattered light in the range between 0° and 180°. The Raman-scattered light is collected by the same microscope objective and a Glan–Thompson prisma selects the component of the scattered light with polarization parallel to that of the incoming excitation light. The scattered light is then coupled into a spectrometer, dispersed by a diffraction grating with 300 lines/mm and focused onto a CCD camera. The low-resolution grating (about 4.5 cm^{-1}) is chosen for two reasons: first, it allows one to capture the full Raman spectrum ranging from 240 to 3,400 cm^{-1} in the same CCD window and, second, reduces the acquisition time, which is essential because of the degradation of the dye under laser illumination.

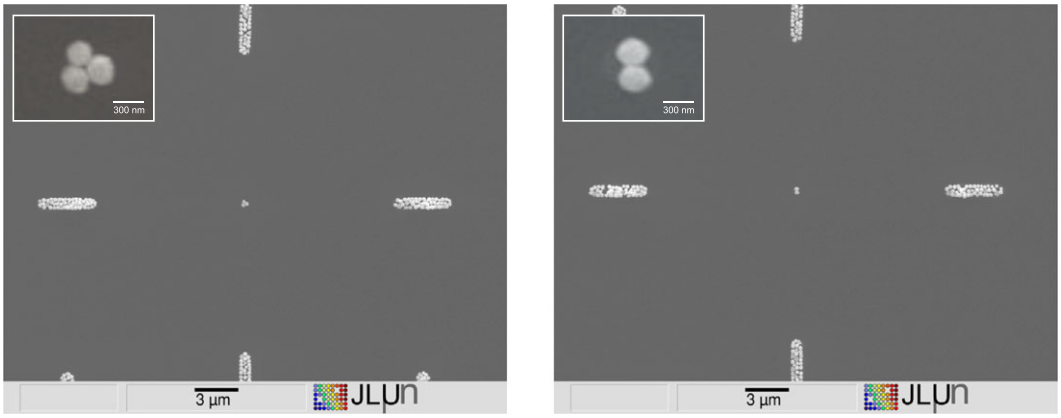

FIGURE 1 Scanning electron microscopic images of nanoparticle arrangements consisting of three (left-hand side) and two (right-hand side) 250 nm gold nanoparticles, that is, trimer and dimer. The markers surrounding the nanoparticle clusters facilitate identification of specific arrangements and their orientation during the Raman experiments [Colour figure can be viewed at wileyonlinelibrary.com]

2.3 | COMSOL simulations

Finite element simulations using COMSOL Multiphysics 5.2 were performed to calculate the electric field enhancement in the hot spot of a dimer in case of incoming light polarized along the dimer axis. We assume that the dimer is formed out of two spherical gold nanoparticles with a diameter of 250 nm and that the dimer is illuminated by a linearly polarized plane electromagnetic wave with a wavelength of 633 nm. To compute the response of the nanoparticles, the refractive index of gold is interpolated from data provided by Johnson and Christy.[25] Scattering boundary conditions are chosen in the simulation. In the physical region of the simulation a "free tetrahedral" meshing with a maximum element size of 13.5 nm is used. We consider the derived electric field distribution converged, when the simulation repeated with the maximum element of the mesh divided in half yields mean deviations of the calculated electric field from the previous simulation with the larger mesh smaller than 0.01%. From the maximum of the electric field in the simulated region, $E_{\max}$ the electric field enhancement factor is approximated by $\tilde{g} = E_{\max}^4$. The simulations are performed for different gap widths d between the nanoparticles.

3 | NANOPARTICLE DIMERS

Raman results obtained on a gold nanoparticle dimer coated in MB and corresponding analysis are presented in Figure 2. The angle α between the linear polarization of the incoming excitation light and the marker was varied in the experiment. The orientation of the dimer axis with respect to the marker is known from the SEM analysis. For this particular specimen, the spectrum taken at $\Delta\alpha = 50°$ corresponds to the situation where dimer axis and polarization direction of the incoming light are parallel. The Raman spectra of the series are characteristic for MB and arise solely from the organic cation. This molecule consists of 38 atoms giving rise to 108 vibrational modes. It possesses C_2 point symmetry, that is, a very low symmetry, thus, yielding Raman-active modes of A and B symmetry only, 54 of each symmetry type. A detailed analysis of the Raman spectrum of MB including assignments of the modes to characteristic vibrations can be found in the literature.[27] In what follows, neither the exact structure of the molecule nor the particular mode patterns of A and B are of importance. For our discussion, we only need to know the form of the two Raman tensors representative for modes of A and B symmetry, as discussed below in more detail. One A-mode and one B-mode at 1,625 and 669 cm^{-1}, respectively, are highlighted in the spectra. They are chosen because they do not overlap with adjacent modes.

The series of Raman spectra in Figure 2a shows distinct variations of intensity with increasing angle, an oscillatory behavior superimposed by a continuous drop in intensity with increasing angle, that is, with prolonged duration of the measurement. The former reflects the characteristics of the hot spot, whereas the latter indicates that the dye molecules degrade under illumination. We will analyse these observations in detail in what follows. Furthermore, A-mode and B-mode possess different Raman tensors, and we will verify whether this has an impact on the angle-dependent mode behavior in this experiment.

3.1 | Degradation of MB

We recorded Raman spectra of a dimer structure coated with MB. The interaction between electromagnetic radiation with MB leads to a degradation of the organic dye.[26] To analyze this effect, the specimen was under continuous illumination at a fixed geometry, and Raman spectra were recorded sequentially and the times logged. It was found

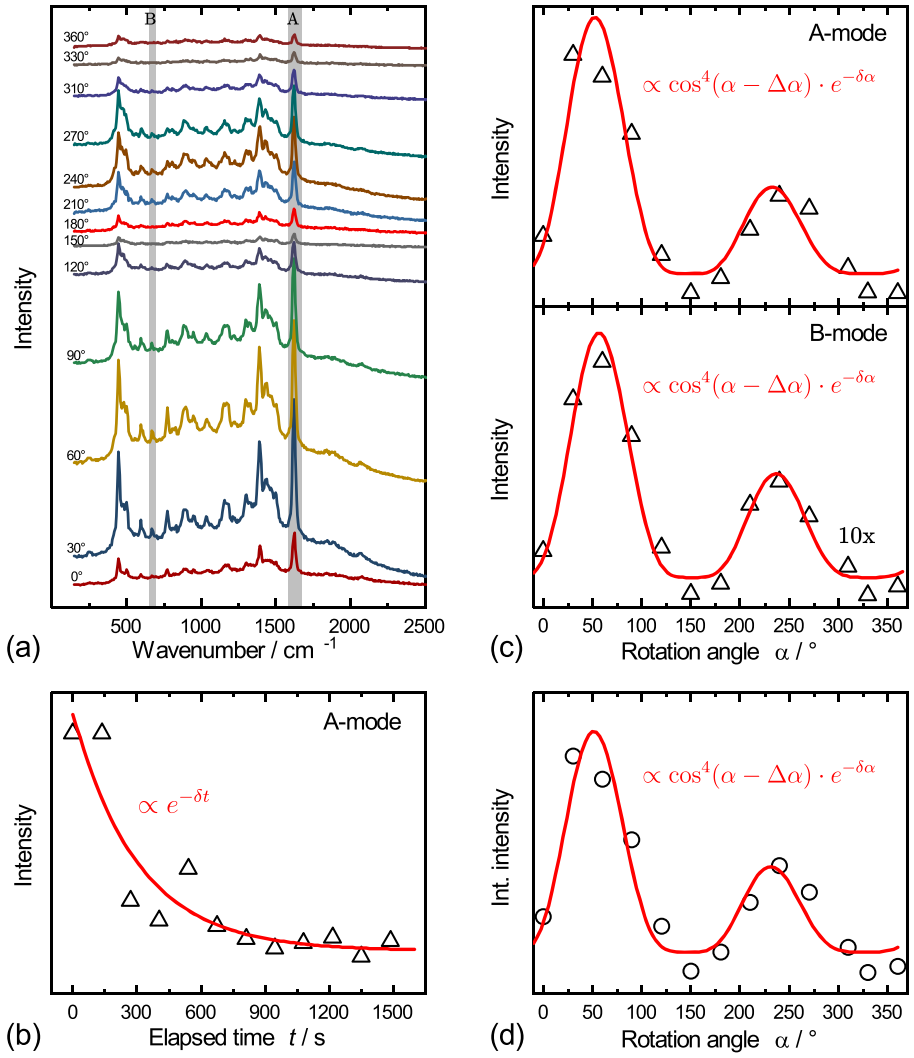

FIGURE 2 (a) Series of Raman spectra of a dimer for different rotation angles of the incoming linear light polarization with respect to the dimer axis. Dimer axis and linear polarization of the excitation light are parallel at $\Delta\alpha \approx 50°$. Only the component of the Raman-scattered light with polarization parallel to that of the incoming excitation light is detected. One of the highlighted peaks corresponds to a Raman mode of A and another to one of B symmetry. (b) Decay of the intensity of the Raman spectra of a dimer structure under laser illumination. The spectra are taken sequentially at different moments in time without altering the measurement geometry. The red solid line represents an exponential decay function fitted to the measurement data. (c) Plots of the Raman intensity as a function of the rotation angle between the polarization of the incoming linearly polarized excitation light and the dimer axis for the mode of A symmetry (upper plot) and the mode of B symmetry (lower plot) marked in (a). The red solid line represents the curve fitted using Equation (1). (d) Total integrated intensity of the Raman spectra in (a) as a function of the rotation angle [Colour figure can be viewed at wileyonlinelibrary.com]

that the intensity of the entire spectrum dropped continuously with increasing duration of the measurement. We show exemplarily in Figure 2b how the intensity of the distinct A-mode at 1,625 cm^{-1} of the MB dye adsorbed onto spherical gold particles forming the dimer decreases with prolonged duration of the measurement. The degradation is well described by an exponential decay. The same behavior manifests itself in the series of spectra obtained as a function of angle because the acquisition time of every spectrum taken adds to the overall duration of illumination of the specimen and the spectra were obtained sequentially starting from 0° to 360°. The laser power was tuned to the lowest possible value of 2 μW. A further reduction of the laser power inhibits the measurement of the Raman spectrum considerably. Although the low laser power helps to reduce degradation of the organic dye molecules, it does not yield a measurable Raman signal in the absence of nanoparticles due to the lack of plasmon-assisted enhancement.

3.2 | Polarization dependence

Here, we analyze the intensity variations in the Raman spectra of the dimer coated with MB in Figure 2a, which occur as a function of angle of the linear polarization of the excitation light with respect to the marker grid, in more detail.

The majority of Raman modes overlap, and the corresponding peaks cannot be disentangled due to the rather low resolution of the spectra compelled by the necessity of short acquisition times to minimize dye degradation. However, the peaks of the A-mode at 1,625 cm^{-1} and of the B-mode at 669 cm^{-1} are sufficiently separated from the neighboring peaks in order to analyze them individually.[27] The intensity of both modes as a function of rotation angle of the polarization is depicted in Figure 2c. Whereas the intensity reaches a maximum when the polarization vector is parallel to the dimer axis, the minima correspond to a perpendicular orientation of polarization vector and dimer axis. According to the E^4 approximation, the Raman intensity scales with

$\cos^4(\alpha - \Delta\alpha)$, where α is the rotation angle and $\Delta\alpha$ denotes the angle where the direction of the polarization and the dimer axis are parallel.[28] It is worth noting that the absolute Raman enhancement in such a hot spot is not solely given by the forth power of the electric field enhancement but will depend also on the number of scatterers as well as on their Raman response. However, as we are only varying the angle of the light polarization with respect to the dimer axis, but always probe the same molecules at the surface, we can assume that, to a first approximation, the difference in Raman signal strength for parallel and perpendicular orientation of the polarization direction with respect to the dimer axis scales with the forth power of the electric field enhancement. Furthermore, as the laser spot is always larger than the gold particle arrangement we will get an additional contribution to the signal due to the dye deposited onto the substrate surface. However, this contribution is independent of α and leads to a constant background, which we subtract from the spectra prior to further analysis.

Figure 2c shows the dependence of the Raman intensity of the A-mode and B-mode and a corresponding fitted curve using

$$I^{\parallel}(\alpha) = g\cos^4(\alpha - \Delta\alpha) \cdot e^{-\delta\cdot\alpha}, \tag{1}$$

where the exponential function accounts for the degradation of the organic dye.[29] The parameter δ is a measure for the degradation, and $g = A\cdot\tilde{g}^4$ is the Raman-enhancement factor where A denotes a Raman specific factor accounting for the Raman response and the number of scatterers. In case of a dimer, it is not possible to distinguish A and $\tilde{g}^4$ in the fitting process. The red solid lines in Figure 2c represent the curve fitted to the data using Equation (1). Excellent agreement is achieved for both modes. Both modes exhibit the same angle dependence despite different mode symmetries and, thus, different Raman tensors. The same angle dependence is also found for the Raman intensity integrated over the spectral range from 240 to 3,400 cm^{-1} as shown in Figure 2d.

3.3 | Symmetry of Raman modes

Here, we explain why the intensities of all Raman modes as a function of the rotation angle between the polarization of the incoming light and the dimer axis exhibit the same behavior for the selected parallel polarization geometry despite the different Raman tensors of modes of different symmetry. If we assume that the MB molecules are oriented randomly inside the hot spot, the total intensity of the Raman signal for a given polarization direction will be obtained by averaging over all possible configurations of the molecule and is proportional to

$$\begin{aligned} I &\propto \int_0^{2\pi}\int_0^{\pi}\int_0^{2\pi} |\mathbf{e}_s^T U^T \mathcal{R} U \mathbf{e}_i|^2 \sin\theta \,\mathrm{d}\phi\,\mathrm{d}\theta\,\mathrm{d}\psi \\ &= \overline{|\mathbf{e}_s^T U^T \mathcal{R} U \mathbf{e}_i|^2} \end{aligned}, \tag{2}$$

where U is the Euler matrix, $\mathcal{R}$ is the Raman tensor, and $\mathbf{e}_i = (\tilde{g}\cos\alpha, \sin\alpha, 0)^T$ is the enhanced electric field vector of the incident light field. The dimer axis is assumed along x-direction, that is, $\alpha = 0°$, and $\tilde{g}$ denotes the electric field enhancement factor for light polarized along the dimer axis. In case of parallel polarizations of incoming and backscattered light, the electric field vector of the enhanced scattered light is also given by $\mathbf{e}_s^T = (\tilde{g}\cos\alpha, \sin\alpha, 0)$. Equation (2) is of general validity.

In case of the organic dye MB, which belongs to the C_2 point group,[27] the Raman tensors are of the form

$$\mathcal{R}_A = \begin{pmatrix} r_1 & 0 & r_4 \\ 0 & r_2 & 0 \\ r_4 & 0 & r_3 \end{pmatrix} \qquad \mathcal{R}_B = \begin{pmatrix} 0 & r_5 & 0 \\ r_5 & 0 & r_6 \\ 0 & r_6 & 0 \end{pmatrix}, \tag{3}$$

for the A-mode and B-mode, respectively.[30] The variables r_i with $i = 1\ldots6$ denote the independent Raman tensor elements, which may be nonzero. Carrying out the calculus according to Equation (2) for both modes and parallel polarizations, as in the experiment, yields

$$\begin{aligned} I^{\parallel}(\alpha) &= f_1^{\parallel}[1 + (\tilde{g}^2 - 1)\cos^2\alpha]^2 \\ &\approx f_1^{\parallel}\tilde{g}^4\cos^4\alpha \end{aligned}, \tag{4}$$

where the approximation holds for $\tilde{g} \gg 1$. The factors $f_1^{\parallel}$ in Equation (4) depend on the nonzero Raman tensor elements and read

$$\begin{aligned} f_1^{\parallel}(R_A) = &\frac{8\pi^2}{15}\left[3\left(r_1^2 + r_2^2 + r_3^2\right) + \right. \\ &\left. + 2(r_1 r_2 + r_1 r_3 + r_2 r_3) + 4r_4^2\right], \end{aligned} \tag{5}$$

$$f_1^{\parallel}(R_B) = \frac{32\pi^2}{15}\left(r_5^2 + r_6^2\right), \tag{6}$$

for modes of A and B symmetry, respectively. It should be noted that, in case of crossed polarizations, the situation is rather complicated, and in particular, the leading term of $I^{\perp}(\alpha)$ for $\tilde{g} \gg 1$ is not simply proportional to $\tilde{g}^4\cos^4\alpha$. A full-depth discussion of this issue without loss of generality can be found in the Supporting Information.

Equation (4) reveals that in case of parallel polarizations, the Raman tensor only affects the amplitude of the oscillations, but has no impact on the functional relationship of the polarization dependence on angle α, which is well approximated by a $\cos^4\alpha$ term. On these grounds, it is justified to use the integrated intensity of the Raman spectra instead of individual modes in studies of enhancement effects of the gold nanoparticle arrangements. The comparison of a corresponding plot in Figure 2d with those of the A-mode and B-mode in Figure 2c confirms this consideration. Furthermore, it indirectly proves that the MB

molecules contributing to the enhanced Raman signal are distributed randomly.

3.4 | Distance dependence of $\tilde{g}$

The electric field enhancement factor $\tilde{g}$ is mainly determined by the distance between the nanoparticles.[17] The simulated dependence of $\tilde{g}^4$ on the gap width d of the dimer serving as master curve in what follows is shown in Figure 3a. The best parametrization for the electric field enhancement $\tilde{g}^4(d)$ is obtained by fitting a stretched exponential function to the logarithm of the simulated electric field enhancement:

$$\ln(\tilde{g}^4(d)) = G_0 \cdot e^{-\left(\frac{d}{\tau}\right)^{\beta}}. \tag{7}$$

Each symbol corresponds to a simulated data point, the fitted curve is given as a solid line. In contrast to a simple exponential function, the stretched exponential function is able to capture the heavy tail of the distribution. The fit yields $G_0 \approx 30.87$, $\tau \approx 3.00$, and $\beta \approx 0.52$.

4 | NANOPARTICLE TRIMERS

A priori, it is not sure that the Raman response of a nanoparticle arrangement exhibiting a number of gaps may be well described by a "sum of independent hot spots." For instance, Le Ru *et al.* showed that the light field, depending of the excitation wavelength used, may induce and favour either surface-plasmon excitations or bulk-plasmon excitations of the same nanoparticle arrangement.[31] Because the two excitation modes exhibit a different polarization dependence, the laser frequency has a crucial impact on the overall polarization dependence observed in experiment. Furthermore, the kind of experiment performed, for example, SERS or absorption/extinction measurements, as well as the nanoparticle configuration itself also determines whether the measurement is more sensitive to surface-like or bulk-like plasmons. Another example was given by Litz *et al.*,[12] who highlighted the difference between localized hot spots and delocalized excitations. Delocalized plasmonic excitations were also observed in highly symmetric arrangements of nanoparticles with diameters below 100 nm.[32] Therefore, in order to verify, whether the Raman response of our trimer structures can be described as a sum of independent hot spots, we have calculated the spatial electric field distributions of a symmetric and an asymmetric trimer for 633 nm excitation. The spatial electric field distributions clearly reveal that the electric field enhancement is strongest in the three gaps between the nanoparticles of the trimer, that is, showing that hot spots have formed. Furthermore, we show that, for each gap, the field enhancement as a function of the angle between the connecting line between the two nanoparticles forming the gap and the direction of the polarization of the incoming excitation light indeed follows a cosine to the power 4 dependence. Details are shown in Figure S3. Thus, we model in the following the Raman response of three spherical gold nanoparticles forming a trimer assuming independent hot spots. The response can be considered the sum of the responses of three independent dimers with different orientations of their axes.

In case of parallel polarization of incoming and scattered light, the trimer Raman response reads

$$\begin{aligned} I^{\parallel}(\alpha) = \big[&g_1\cos^4(\alpha) + g_2\cos^4(\alpha+\gamma_3) + \\ &+ g_3\cos^4(\alpha-\gamma_2)\big] \cdot e^{-\delta\cdot\alpha}, \end{aligned} \tag{8}$$

where γ_2 and γ_3 are the angles between the dimer axes and $\alpha = 0$ corresponds to the polarization of the light parallel to the axis of the dimer formed by nanoparticles 2 and 3, as shown in Figure 3b. The parameters g_1, g_2, and g_3 are the Raman-enhancement factors of the three dimer hot spots. Assuming that the coverage of the trimer with the dye is homogeneous, it holds for $i = 1, 2, 3$ that $g_i = A \cdot \tilde{g}_i^4 = A \cdot \tilde{g}_i^4(d_i)$ where $\tilde{g}_i^4(d_i)$ is given by Equation (7). The distance d_i between two adjacent nanoparticles with radii R_j and R_k is related to the opposite angle γ_i in the triangle by

$$x_{sc} = \frac{d_i + R_j + R_k}{\sin(\gamma_i)}, \tag{9}$$

where x_{sc} is the same for all three hot spots of a trimer. The dependence $I^{\parallel}(\alpha)$ is obtained by combining the model of independent hot spots represented by Equation (8) with Equation (9) and the parameterization $\tilde{g}^4(d)$ according to Equation (7):

$$\begin{aligned} &I^{\parallel}(\alpha) = \\ &A\left[\tilde{g}_1^4(d_1)\cos^4(\alpha) + \tilde{g}_2^4(d_2)\cos^4(\alpha+\gamma_3) + \right. \\ &\left. + \tilde{g}_3^4(d_3)\cos^4(\alpha-\gamma_2)\right] e^{-\delta\cdot\alpha}, \end{aligned} \tag{10}$$

where, making use of $d_1 = \sin(\gamma_1) - R_2 - R_3$ and corresponding expressions obtained by cyclic permutation of the indices,

$$\ln \tilde{g}_i^4 = \exp\left[-\left(\frac{\sin(\gamma_i)x_{sc} - R_j - R_k}{\tau}\right)^{\beta}\right], \tag{11}$$

for $(ijk) = (123), (231)$, and (312).

To verify the simulated master curve of electric field enhancement $\tilde{g}^4(d)$, a fit of Equation (10) to the angle variation of the integrated intensity of the Raman spectra belonging to nanoparticle trimers is performed. The number of variables in the fitting process is drastically reduced by exploiting the assumption of similar triangles in describing the trimer's Raman response. The angles γ_i and the radii R_i are obtained from SEM images of the clusters by approximating the nanoparticles by spheres

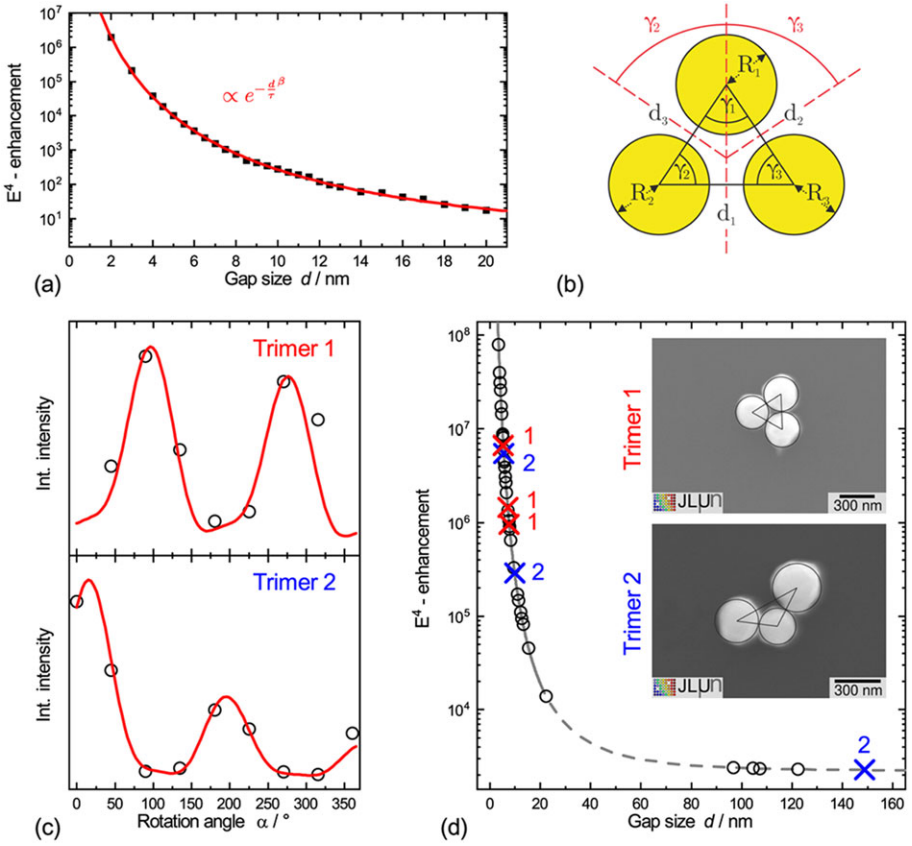

FIGURE 3 (a) Electric field enhancement $\tilde{g}^4$ between adjacent spherical gold nanoparticles as a function of gap width d (filled squares) derived by finite element simulations using COMSOL and serving as master curve in the analysis. The red solid line represents a fitted curved of $\ln \tilde{g}$ with a stretched exponential function. (b) Schematic representation of a nanoparticle trimer with the definition of angles and lengths used in the analysis. (c) Integrated intensity as a function of the rotation angle of the linear polarization of the excitation light with respect to the trimer arrangement for two different trimers. The red solid lines represent the fitted curve based on Equation (10). (d) Parametrization of the master curve of the electric field enhancement (black line) based on Equation (7). The six pairs $(d, \tilde{g})$ used in the fitting of angle-dependent Raman intensities of Trimer 1 and 2 are given as red and blue crosses. The open circles denote additional pairs $(d, \tilde{g})$ probed in the fitting of the eleven trimers shown in Supporting Information. Inset: SEM images of Trimers 1 and 2 where the black circles visualize how the shape of nanoparticle trimer is approximated in the fitting process [Colour figure can be viewed at wileyonlinelibrary.com]

and analyzing the triangle formed by the nanoparticles' centers. Thus, we use only the scaling parameter x_{sc}, the Raman-response parameter A, and the degradation coefficient δ as variables in the fitting process. The underlying assumptions, namely, the independence of the hot spots and the random orientation of the molecules, are justified by the excellent agreement between the curves fitted with Equation (10) and the experimental data.

The results of the curve fitting are presented in Figure 3c. The integrated intensity of Raman spectra as a function of the rotation angle is depicted for two trimers. The fitted curves are represented by red lines. SEM images of the two trimers are presented in the inset of Figure 3d . The nanoparticles of Trimer 1 are arranged symmetrically. The difference in the three dimer gaps d_i is therefore small. The anisotropic arrangement of Trimer 2 is characterized by one large gap with a width of approximately 150 nm, whereas the other gaps are probably between 5 and 10 nm wide. The distances d_i obtained for both trimers by the fitting process are in concordance with the SEM images discussed. The shapes of the trimer arrangements used in the modelling are plotted to scale on top of the corresponding SEM images and show a good agreement within the experimental uncertainty. Corresponding $(d, \tilde{g}^4)$ pairs are marked on the simulated master curve in Figure 3d. The black line in the figure represents the parametrization of the master curve obtained by Equation (7). Because no simulations have been performed beyond a separation of 20 nm, the region, in which the line is dashed, represents an extrapolation from the simulation results using the stretched exponential according to Equation (7).

The good agreement between the trimer shapes modeled and those obtained by SEM is remarkable. A verification of the width of the smaller gaps by SEM is not possible due to the resolution of the SEM. However, the agreement between the modeled shape and the SEM image in case of both trimers is a confirmation that the simulated master curve of the electric field enhancement $\tilde{g}^4$ is realistic.

In total, we have analyzed 11 more trimers in the same fashion in order to verify the $\tilde{g}(d)^4$ master curve. It should be noted that we were able to describe the angle-dependent Raman data of all 13 trimers using the similar values of

A and δ, reflecting that all trimers have similar densities of scatterers in their hot spots, as anticipated, due to the coating with dye molecules according to the same preparation protocol. The results are shown in Figures S1 and S2. Thus, we have probed almost forty positions $(d, \tilde{g}^4)$ on the master curve indicated by the crosses (data corresponding to Trimers 1 and 2) and open circles (data corresponding to the Trimers 3 to 13 discussed in Supporting Information) in Figure 3d. Our modelled results somewhat suggest that deviations of the nanoparticle's shape from a perfect sphere play a minor role in determining the strength of the enhancement, although it is well known that edges and kinks on the nanoparticle surface may modify the electromagnetic near-field distribution.[33] To further analyze this effect, we performed additional finite element simulations, not shown here, which confirmed that the impact of the nanoparticle shape on the Raman intensity is orders of magnitude lower than the influence of the gap width between the nanoparticles. In this context, it is particularly worth noting that a further confirmation of the calculated enhancement on gap width is given by the finding that the widths of the large gaps (which are accessible by SEM) of the nanoparticle trimers in Figure S2 are in good agreement with the width values obtained by the curve fitting.

The strength of the triangulation approach is the strong restriction imposed on $\tilde{g}_1$ to $\tilde{g}_3$ by assuming similar triangles in the fitting which due to the strongly and continuously decreasing slope of the master curve $\tilde{g}^4$ with increasing d enforces unique solutions of (d_1, d_2, d_3) in the fitting of the experimental data by Equation (10). If a second solution (d_1', d_2', d_3') yielding the same best fit existed, it would have to fulfill the following criteria: (a) constant $x_{sc} = d_i'/d_i$ for $i = 1, 2, 3$ due to the assumption of similar triangles describing the trimer and (b) constant $C = (\tilde{g}_i'/\tilde{g}_i)^4$ for $i = 1, 2, 3$ in order to yield a parameter A' such that the same best fit to the experimental data is obtained using Equation (10), which requires relation $A = A' \cdot C$ to hold. This is not possible because

$$\begin{aligned}\ln \tilde{g}'^4 &= \ln\left(\tilde{g}^4(d')\right) = \ln\left(\tilde{g}^4(x_{sc} \cdot d)\right) \\ &= \exp\left[-\left(\frac{x_{sc} \cdot d}{\tau}\right)^{\beta}\right] \\ &= \exp\left[-\left(\frac{d}{\tau}\right)^{\beta}\right] \cdot \exp\left[-\left(\frac{d}{\tau}\right)^{\beta}\right]^{x_{sc}^{\beta}-1} \\ &= \ln\left(\tilde{g}^4(d)\right) \cdot \exp\left[-\left(\frac{d}{\tau}\right)^{\beta}\right]^{x_{sc}^{\beta}-1} = \ln\left(\tilde{g}^4(d)\right) \cdot S(d),\end{aligned} \tag{12}$$

that is, the factors S and, thus, C, depends on d. Accordingly, requirement (b), the existence of a constant C, cannot be fulfilled.

5 | SUMMARY AND CONCLUSIONS

In summary, we fabricated triangular arrangements of gold nanoparticles (i.e., trimers) by a mensicus-force approach on lithographically prepatterned substrates and dip-coated them with MB dye serving as Raman probe. All trimers were mapped carefully in terms of diameters and angles between the nanoparticles. We performed polarization-dependent Raman-spectroscopic measurements as a function of angle on 13 individual trimers. The angle dependence of the enhanced Raman intensity of the dye coating was analyzed assuming an independence of the enhancement action of the three interparticle gaps occurring in a trimer and a random arrangement of dye molecules within the particle gap. A formula for the intensity as a function of angle is derived, which accounts for the fixed trimer geometry and, thus, requires only one scaling factor for all three interparticle gaps instead of one for each gap in case of dimers. The angle-dependent intensity of each trimer was fitted using the same master curve of the electric field enhancement versus interparticle gap width derived by finite element simulations. A consistent description of the Raman intensity behavior of all trimers studied is achieved and in excellent agreement with the analysis of the corresponding scanning electron microscopic images. Furthermore, we prove theoretically that, in case of randomly orientated molecules inside a dimer resonator, the Raman intensity of all modes independent of mode symmetry is dominated by a $\cos^4\alpha$ term where α is the angle between dimer axis and polarization of the incoming light in case of parallel polarizations of incoming and scattered light. Based on this result, we demonstrate that the assumption of a random orientation of the dye molecules is in accordance with the intensity behavior measured for the Raman modes of different symmetry and for the integral Raman intensity. We can conclude that the electric field enhancement between adjacent nanoparticles and its impact on the Raman enhancement in resonator structures consisting of arrangements of spherical gold nanoparticles is well described by Maxwell's theory. In case of the nanoparticle arrangements studied, which consisted of gold nanoparticles with diameters of about 250 nm, the Raman response is well described by a sum of independent hot spots corresponding to the gaps between adjacent nanoparticles of the arrangement. The triangulation approach described may offer means of separating chemical and field enhancement contributions to the Raman enhancement, which will considerably contribute to a better understanding of SERS and TERS techniques and their applications.

ORCID

Katharina Dort https://orcid.org/0000-0003-0849-8774
Kathrin Kroth https://orcid.org/0000-0003-0736-781X
Peter J. Klar https://orcid.org/0000-0002-4513-0330

REFERENCES

[1] D. L. Jeanmaire, R. P. Van Duyne, *J. Electroanal. Chem. Interfacial Electrochem.* **1977**, *84*, 1.
[2] D. A. Stuart, J. M. Yuen, N. Shah, O. Lyandres, C. R. Yonzon, M. R. Glucksberg, J. T. Walsh, R. P. Van Duyne, *Anal. Chem.* **2006**, *78*, 20.
[3] E. C. Dreaden, A. Alkilany, X. Huang, C. J. Murphy, M. A. El-Sayed, *Chem. Soc. Rev.* **2012**, *41*, 7.
[4] Y. Li, Q. Wei, F. Ma, X. Li, F. Liu, M. Zhou, *Acta. Pharm. Sin. B.* **2018**, *8*, 3.
[5] K. Kneipp, Y. Wang, H. Kneipp, L. T. Perelman, I. Itzkan, R. R. Dasari, M. S. Feld, *Phys. Rev. Lett.* **1997**, *78*, 9.
[6] S. Nie, S. R. Emory, *Science* **1997**, *275*, 5303.
[7] J. Jiang, K. Bosnick, M. Maillard, L. Brus, *J. Phys. Chem. B.* **2003**, *107*, 37.
[8] U. Kreibig, M. Vollmer, *Optical Properties of Metal Clusters*, Springer, Berlin Heidelberg **1995**.
[9] P. Nordlander, C. Oubre, E. Prodan, K. Li, M. I. Stockman, *Nano Lett.* **2004**, *4*, 5.
[10] P. G. Etchegoin, C. Galloway, E. C. Le Ru, *Phys. Chem. Chem. Phys.* **2006**, *8*, 22.
[11] J. Zuloaga, E. Prodan, P. Nordlander, *Nano Lett.* **2009**, *9*, 2.
[12] J. P. Litz, J. P. Camden, D. J. Masiello, *Phys. Chem. Lett.* **2011**, *2*, 14.
[13] J. A. Creighton, *Surf. Sci.* **1983**, *124*, 1.
[14] L. Zhao, L. Jensen, G. C. Schatz, *J. Am. Chem. Soc.* **2006**, *128*, 9.
[15] D. A. Long, *Raman Spectroscopy*, McGraw-Hill, New York **1980**.
[16] D. P. Strommen, *J. Chem. Educ.* **1992**, *69*, 10.
[17] P. K. Jain, W. Huang, M. A. El-Sayed, *Nano Lett.* **2007**, *7*, 7.
[18] Z. Yang, J. Aizpurua, H. Xu, *J. Raman Spectrosc.* **2009**, *40*, 10.
[19] L. Meng, M. Sun, *Photonics Res.* **2017**, *5*, 6.
[20] B. Pettinger, B. Ren, G. Picardi, R. Schuster, G. Ertl, *J. Raman Spectrosc.* **2005**, *36*, 6.
[21] J. Gersten, A. Nitzan, *J. Chem. Phys.* **1980**, *73*, 7.
[22] Y. Cui, M. T. Björk, J. A. Liddle, C. Sönnichsen, B. Boussert, A. P. Alivisatos, *Nano Lett.* **2004**, *4*, 6.
[23] A. Fabian, M. T. Elm, D. M. Hofmann, P. J. Klar, *J. Appl. Phys.* **2017**, *121*, 22.
[24] A. Fabian, M. Czerner, C. Heiliger, M. T. Elm, D. M. Hofmann, P. J. Klar, *Phys. Rev. B* **2018**, *98*, 5.
[25] P. B. Johnson, R. W. Christy, *Phys. Rev. B.* **1972**, *6*, 12.
[26] P. S. Dittrich, P. Schwille, *Appl. Phys. B: Lasers Opt.* **2001**, *73*, 8.
[27] S. Dutta Roy, M. Ghosh, J. Chowdhury, *J. Raman Spectrosc.* **2015**, *46*, 5.
[28] H. Xu, M. Käll, *Phys. Chem. Chem. Phys.* **2003**, *4*, 9.
[29] P. G. Etchegoin, E. C. Le Ru, R. C. Maher, L. F. Cohen, *Phys. Chem. Chem. Phys.* **2007**, *9*, 35.
[30] R. Loudon, *Adv. Phys.* **1964**, *13*, 52.
[31] E. C. Le Ru, C. Galloway, P. G. Etchegoin, *Phys. Chem. Chem. Phys.* **2006**, *8*, 26.
[32] J. Ye, F. Wen, H. Sobhani, J. B. Lassiter, P. Van Dorpe, P. Nordlander, N. J. Halas, *Nano Lett.* **2012**, *12*, 3.
[33] K. L. Kelly, E. Coronado, L. L. Zhao, G. C. Schatz, *J. Phys. Chem. B.* **2003**, *107*, 3.

SUPPORTING INFORMATION

Additional supporting information may be found online in the Supporting Information section at the end of the article.

How to cite this article: Dort K, Kroth K, Klar PJ. A surface-enhanced Raman-spectroscopic study: Verification of the interparticle gap dependence of field enhancement by triangulation of spherical gold nanoparticle trimers. *J Raman Spectrosc*. 2019;50: 1807–1816. https://doi.org/10.1002/jrs.5728